

Experimental demonstration of sequential excitation scheme for H^- laser assisted charge exchange

Alexander Aleksandrov[✉], Sarah Cousineau, Timofey Gorlov, Yun Liu[✉], Abdurahim Oguz[✉],
Andrei Shishlo, and Alexander Zhukov[✉]

Oak Ridge National Laboratory, Oak Ridge, Tennessee 37830, USA

Martin Kay[✉]

University of Tennessee, Knoxville, Tennessee 37996, USA



(Received 28 December 2022; accepted 27 March 2023; published 26 April 2023)

Charge exchange injection is the standard mechanism used to accumulate short, intense pulses of proton beams from an H^- injector into a synchrotron. Historically, this process has relied on injection foils to remove the two electrons from the H^- , a technique that has been successfully employed for beam powers up to 1.4 MW. However, such foils are known to sublimate beyond a threshold beam power density, requiring the development of another stripping technology that does not have the same limitation. This work reports on the experimental development of laser assisted charge exchange (LACE) as a mechanism for replacing the foils. In the present work, a method of laser assisted charge exchange that is scalable to full duty factor operation is experimentally demonstrated. The method, termed “sequential resonance excitation,” relies on a two-step quantum excitation of the electron from the ground state to the excited state. Compared with previously reported LACE experiments that utilized a single-step excitation, this method significantly reduces the required peak laser power, allowing for scalability to millisecond-long H^- pulses with conventional laser technology.

DOI: [10.1103/PhysRevAccelBeams.26.043501](https://doi.org/10.1103/PhysRevAccelBeams.26.043501)

I. INTRODUCTION

Accumulation of intense, short pulse proton beams in a synchrotron is typically accomplished through charge exchange injection using stripper foils [1]. The stripper foil implementation of charge exchange has been demonstrated to work with beam powers up to 1.4 MW but has known limitations, including beam scattering leading to high levels of beam loss and radiation [2] and foil heating resulting in sublimation beyond a threshold beam power density. Recent measurements have determined that the practical beam power density limit for foils due to sublimation is within a factor of 5 of existing beam power densities [3]. The beam power limitation on traditional solid foils is not unique to H^- charge exchange injection in proton synchrotrons. For instance, high-power ion facilities are now using alternative liquid-based methods of charge exchange to overcome similar thermal limitations with traditional stripping methods [4].

The method of laser assisted charge exchange (LACE) has been under development over the past two decades as an alternative material-free method of H^- charge exchange for beam injection into a synchrotron. This method replaces the foil with a laser and magnet ensemble. In this scheme, the incoming H^- beam is passed through a dipole magnet which strips the more loosely bound electron via Lorentz stripping. A laser is then used to excite the remaining electron from the ground state to a higher quantum state, at least $n = 3$, whereby it can be removed by passing through another magnetic field before it decays back to the ground state. The excitation of the electron by the laser is a resonance phenomenon that requires precisely the right photon frequency, dependent on the ion beam energy according to

$$f_{\text{BeamFrame}} = \gamma(1 + \beta \cos \alpha) f_{\text{LabFrame}}, \quad (1)$$

where γ and β are relativistic factors, α is the crossing angle between the laser and ion beam, $f_{\text{BeamFrame}}$ is the photon frequency in the ion frame of reference, and f_{LabFrame} is the photon frequency in the laboratory frame. Other similar approaches to charge exchange with lasers are under consideration. Most notably, there is a development effort to directly photoionize both electrons in the H^- beam, thus converting H^- to protons without the use of any

Published by the American Physical Society under the terms of the [Creative Commons Attribution 4.0 International license](https://creativecommons.org/licenses/by/4.0/). Further distribution of this work must maintain attribution to the author(s) and the published article's title, journal citation, and DOI.

magnets [5,6]. This method requires substantially more laser power.

The LACE method has undergone experimental evolution at the Spallation Neutron Source (SNS) accelerator [7] thus far in three steps: First, a proof of principle experiment demonstrated high-efficiency stripping of a 6 ns H^- pulse using 10 MW of peak laser power [8]. A follow-up experiment employed ion and laser beam optics and timing manipulations to extend the stripped pulse length by a factor of 1000 to 10 μ s [9,10]. From there, another factor of 100 in stripped pulse duration was still required to reach full duty factor implementation. However, the average laser power required for this extension was not feasible with existing laser technology. To overcome the laser power limitation, a variant of the original method was proposed in Ref. [11] which splits the multilevel single-step excitation of the electron into smaller substeps. This method, called “sequential resonance excitation,” reduces the required laser power to achieve full duty factor stripping to within currently available laser technology and provides additional flexibility on the choice of laser wavelength for each substep.

This paper reports on the results of the third experimental step in the LACE development program, which demonstrates the method of sequential resonance excitation. Reference [11] identifies a particular sequential resonance excitation configuration that can utilize the existing hardware infrastructure from the previous SNS stripping demonstration with minor modifications. A consequence of utilizing existing hardware rather than building a new experimental chamber is that high-efficiency stripping for this particular configuration is not achievable or expected. As described below, the best achievable stripping efficiency according to models is 3%–15%. Thus, the goal of this experiment is not to produce high stripping efficiency with sequential resonance excitation but rather to match the simulated prediction in order to validate the approach and the physics. After successful accomplishment of this goal, a planned follow-up experiment will be based on a new experimental vessel with optimized configuration to produce high-efficiency (>95%) stripping.

Some additional challenges of this experiment, described further below, are the need to properly align two laser and ion beam interactions (as opposed to one in the previous single-step experiments) and to perform the second alignment of the excited neutral atom H^{0*} without diagnostics that rely on the charge of the beam. Additionally, pulse to pulse alignment of the ion and laser beam is challenging due to laser pointing instability resulting from the long transport line of the laser through the tunnel; this was also a challenge in the previous experiment. The full experimental setup and results are described below, beginning with a description of the ion and laser beam parameters in Sec. II. A description of the beam diagnostics that were used or developed for the

experiment is given in Sec. III, the laser beam delivery system in Sec. IV, and finally the results in Sec. V. Future plans are discussed in Sec. VI.

II. SELECTION OF ION AND LASER BEAM PARAMETERS

A dedicated experimental station was built at the SNS 1 GeV high-energy beam transport (HEBT) beam line for the second phase of the LACE R&D study (macropulse stripping demonstration). This station includes a high-power UV laser, a laser beam transport line with the final optics and a stabilization system, a vacuum vessel with the stripping magnets, and beam diagnostics [10]. The hardware design was optimized to achieve maximum stripping efficiency using single-step excitation of the H^0 atom from the ground state $n = 1$ to $n = 3$. It would require significant time and cost to build a completely new setup optimized for the sequential excitation scheme; therefore, the approach for demonstrating the feasibility of the sequential excitation was to minimally modify the existing hardware. The parameters that cannot be changed are the laser wavelength $\lambda = 355$ nm, defined by the existing laser and transport line; the laser and ion beam intersection angles, $\alpha_1 = 37.5^\circ$ and $\alpha_2 = 142.5^\circ$, defined by the geometry of the vacuum chamber; and the strength of the stripping magnets made of a permanent magnet material. The maximum stripping efficiency achievable within these constraints is below the desirable >95% level but is sufficient for experimental demonstration of the method feasibility and for developing tuning procedures. A layout of the SNS LACE experimental vessel is shown in Fig. 1.

A. First-step excitation from $n = 1$ to $n = 2$

With the laser wavelength and the interaction angle fixed, the only available free parameter to adjust the photon

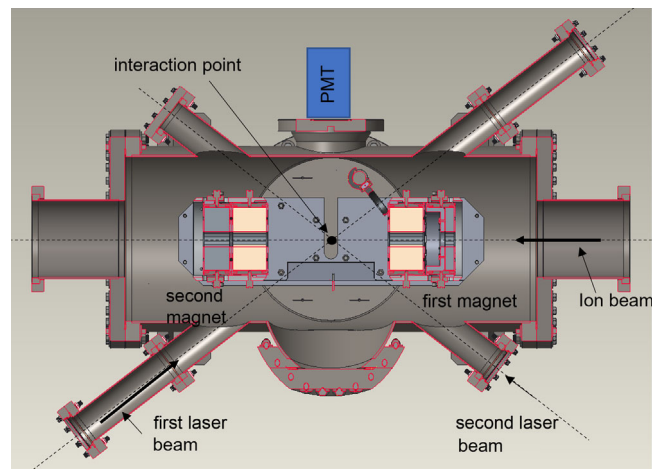


FIG. 1. Layout of the SNS LACE experiment interaction region optimized for single-step excitation experiment.

energy in the ion rest frame, according to Eq. (1), is the ion beam energy. The required energy of 718 MeV is easily achievable by properly tuning the SNS linac. This energy is high enough for efficient 100% stripping of the first electron in the existing fixed field magnet. However, the magnetic field gradient was optimized to minimize the vertical emittance increase of a 982 MeV beam in the single-step excitation experiment and is not optimal for the 718 MeV beam. In addition, the emittance of the lower-energy beam is larger proportionally to $\beta\gamma$. The combined result of the two effects sets a limit for the minimum vertical H^0 beam size at the interaction point. The minimum beam size that can be achieved with the 718 MeV beam was ~ 0.5 mm compared to ≈ 0.1 mm in the previous experiments with 982 MeV beam. The vertical size of the first laser beam is chosen to completely overlap the ion beam. The laser power density is inversely proportional to the vertical laser beam size, which results in a 50% reduction of the effective laser power.

B. Excitation from $n=2$ to higher levels

After the beam energy is selected for resonant excitation from $n=1$ to $n=2$, the required angle of the second laser beam is solely determined by the second excitation scheme. According to Eq. (1), the required angle is 147.4° for the resonant excitation from $n=2$ to $n=3$, and the required angle is 135.4° for $n=2$ to $n=4$. While both angles are close to 142.5° allowed by the existing vacuum chamber, they are not sufficiently close to bring the laser beam to the interaction point without modification of the vacuum chamber. An angle-adapting optical setup has been designed to realize the desired laser-ion interaction angle in the existing vacuum chamber. The optical setup is shown in Fig. 9 and is described in Sec. IV. The current modification can achieve only the excitation from $n=2$ to $n=4$, as the excitation from $n=2$ to $n=3$ will require the angle-adapting optical setup positioned too close to the beam line. Unfortunately, the efficiency of transition from $n=2$ to $n=4$ is ≈ 8 times smaller than from $n=2$ to $n=3$ for the same laser power [11], which is the biggest factor in the stripping efficiency loss due to the nonoptimal geometry of the existing experimental vessel.

C. Mitigation of the ion beam momentum and angular spread

Excitation of the hydrogen atom is a highly efficient process when the resonant conditions are met exactly, which can be done only for a moving hydrogen atom with a given energy and trajectory angle. Unfortunately, particles in a real accelerator have a spread of energies and angles far exceeding the width of the atomic resonance, and, thus, each particle perceives a different wavelength of laser light. Per Eq. (1), the dependence of the transformed photon wavelength on the incident angle α is nonlinear. The left

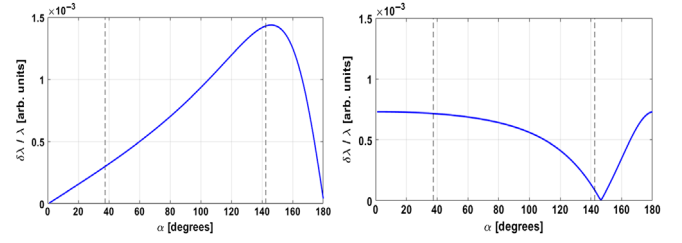


FIG. 2. Deviation of the laser light wavelength in the ion beam reference frame due to 1 mrad deviation of the crossing angles (left) and 1×10^{-3} deviation of the ion energy (right) versus the crossing angle.

plot in Fig. 2 shows the deviation of the photon wavelengths from the resonance in the rest frame of a 718 MeV reference particle resulting from the ion beam horizontal angle deviation from zero. The right plot in Fig. 2(b) shows the dependence of the deviation of the photon wavelengths due to the ion beam energy deviation from the design energy. The first and second laser beam crossing angles in the experiment are shown by the dashed lines. The effect of the energy spread is dominant for the excitation from $n=1$ to $n=2$ by the laser beam at 37.5° and is much smaller for the $n=2$ to $n=4$ transition by the laser beam at 135.4° . However, the effect of the angular spread is large for the second transition; therefore, both laser beams need to have a divergence on the order of a few milliradians to provide resonant conditions for all particles in the beam. Adding divergence to the laser beam further reduces the effective laser power [12].

The optimal parameters for the laser beam size and divergence were found using a computer simulation of the sequential excitation process [13,14]. The main ion and laser beams parameters used in the simulation and experiment are shown in Tables I and II.

The simulation code [13] is based on the transition efficiency calculation formalism for a single particle described in Refs. [11,12]. The electric field of the laser beam in the particle rest frame is calculated using the laser beam parameters from Table II. The particle energy

TABLE I. Ion beam parameters in the experiment.

Parameters	Value	Comment
Current	30 mA	
Energy	718.5 MeV	
Pulse duration	1 μ s	
Pulse repetition rate	1–5 Hz	
Transverse emittance, rms	0.5 μ m	Measured
Vertical size at IP, rms	0.5 mm	Measured
Horizontal size at IP, rms	1.0 mm	Measured
Momentum spread, rms	5×10^{-4} – 10^{-3}	From model
Horizontal angular spread, rms	1.0 mrad	From model

TABLE II. Laser beam parameters in the experiment.

Parameter	Value	Comment
Wavelength	355 nm	
Pulse width (FWHM)	50 ns	
Peak power at IP	0–1.3 MW	Total for two beams, with arbitrary split
First beam vertical size at IP, rms	0.6 mm	Measured
First beam horizontal divergence	1.14 mrad	Measured
Second beam vertical size at IP, rms	0.9 mm	Measured
Second beam horizontal divergence	0.08 mrad	Measured
Expected stripping efficiency	0.03–0.15	Simulation, range is due to the ion beam momentum and angular spread uncertainty

and angles are sampled from a Gaussian distribution with the rms bunch parameters from Table I. The additional vertical angle and displacement introduced by stripping the first electron in the magnet are also taken into account. The average excitation efficiency of all particles is what we call the expected “stripping efficiency,” because all electrons in the excited state $n = 4$ are detached by the second stripping magnet. The main uncertainty in calculating the expected stripping efficiency is due to not precisely known energy and horizontal angular spreads of the bunch, which are not measured directly but derived from the linac model. It is assumed in the simulations that both the laser beam centers are aligned with the ion beam center. Experimentally, this is achieved through a tuning process described in the next section. The laser position jitter is not taken into account explicitly, because we assume it can be minimized to negligible values in a properly implemented laser transport line. We discuss the uncertainty of the simulated efficiency and the jitter effect in more details in the Appendix.

III. BEAM DIAGNOSTICS

The previous LACE experiments with one-step excitation used a minimum set of dedicated diagnostics: a beam current monitor (BCM) before the first stripping magnet, a beam current monitor after the second stripping magnet, and a wire scanner at the interaction point. The vertical overlap of the laser and the ion beams was roughly set using the wire scanner, and the crossing angle was tuned by observing the proton current in the second BCM. Setting up the two-step excitation scheme is much more complex, because the first transition does not result in the conversion of the excited atom to a proton and, therefore, cannot be tuned by scanning the crossing angle while observing the downstream BCM proton current signal. Finding the correct crossing angle for each laser requires searching in two-dimensional space. To facilitate the experiment setup, two dedicated diagnostics were added, a fluorescence monitor and a high-sensitivity beam current monitor.

A. The fluorescence monitor

The $n = 2$ level of the excited hydrogen atom is not stable and returns to the $n = 1$ state emitting a photon with wavelength $\lambda = 121$ nm in the atom rest frame. It was proposed in Ref. [11] to use this emission as a measure of the first-step excitation efficiency. In the laboratory frame, the wavelength of the emitted photon depends on the observation angle as shown in Fig. 3. A Hamamatsu R6834 photomultiplier tube (PMT) was placed at an available view port at 90° relative to the beam trajectory as shown in Fig. 9. The fluorescence wavelength of $\lambda = 220$ nm in the laboratory rest frame is convenient for detection, because this UV light is not absorbed by fused silica glass of the vacuum window, is detectable by readily available PMTs, and is sufficiently separated from the laser wavelength. A narrow band optical filter (Andover Corporation 228FS25-25) was added between the view port and the PMT to reduce the parasitic signal from the laser light reflections. The fluorescence monitor was successfully used to observe the $n = 1$ to $n = 2$ excitation in the initial experiments when the second laser beam was not yet available. A typical fluorescence signal is shown in Fig. 4.

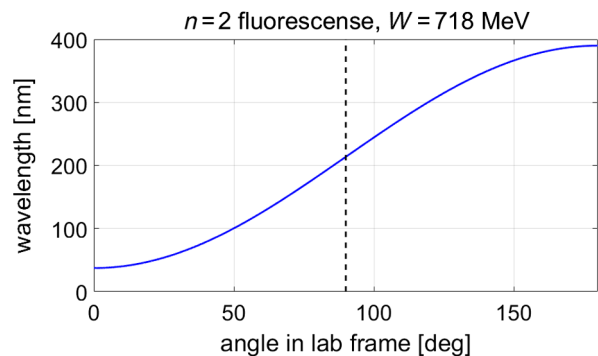


FIG. 3. Dependence of the luminescence wavelength in the laboratory frame of reference upon the detection direction angle. The dashed line shows the PMT angle of view during the experiment.

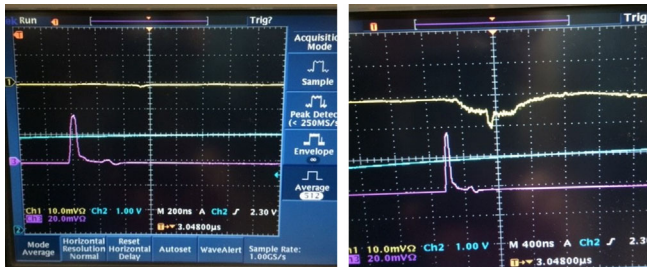


FIG. 4. An oscilloscope screen shot of the fluorescence detector signal. The left panel shows signals with the laser beam open but the ion beam blocked. The right panel shows signals with both beams open. The top trace is the PMT signal; the bottom trace is a photodiode signal for triggering. A weak laser-induced background is seen in the left panel. The right panel shows the radiation background during the beam pulse and the fluorescence signal in the middle of the pulse.

The signal induced in the PMT by the ions lost on the stripping magnet aperture significantly limited the sensitivity of the detector. This problem was not anticipated, because the beam loss at the experiment location is typically very low during normal operation when the stripping magnets are retracted from the beam path. Another problem discovered after several months of operation was a gradual increase of the laser-induced signal in the detector. The exact cause is not known, but one possibility is optical filter quality degradation due to the radiation damage from beam loss. Eventually, the laser light transmission became so large that the detection of the fluorescence became impossible.

Instead of replacing the filter, the detector was repurposed for observing the laser light reflected from the wire scanner wire. This allowed finding the laser beam vertical positions relative to the ion beam position quickly and reliably. The position of each of the three beams (ion beam, first laser beam, and second laser beam) is found by performing the wire scan with the other two beams blocked. In the case of the ion beam, the wire scanner collects the charge intercepted by the wire. In the case of either of the two laser beams, the PMT detects the light reflected by the wire. An example of the measured laser beam profile is shown in Fig. 5.

B. The high-sensitivity beam current monitor (HSBCM)

In the previous LACE experiments, a modification of the standard SNS BCM, based on a current transformer, was used to measure the incoming H^- current and proton current after the interaction point. The minimum beam current detectable above the noise floor was in the range of hundreds of microamperes, which corresponds to the sensitivity limit of about 1% for the stripping efficiency. A new current monitor with much higher sensitivity and wider range was developed for the sequential excitation experiment to allow detection of the weak initial interaction

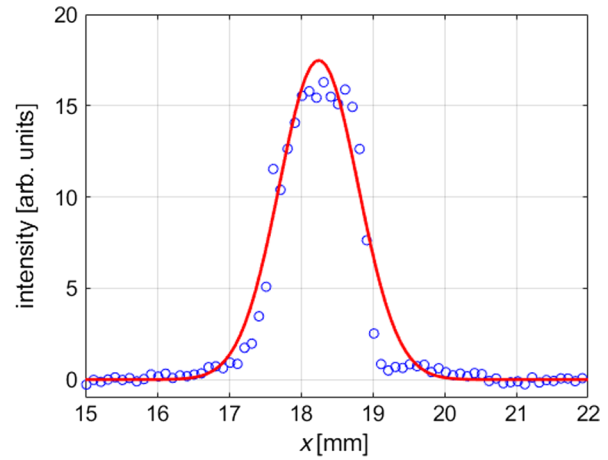


FIG. 5. The laser beam profile measured using the wire scanner and PMT arrangement.

and then gradual optimization of all the parameters to achieve the maximum efficiency. A standard SNS strip-line beam position monitor (BPM) [7] downstream of the interaction point was reconfigured for this purpose. The beam-induced signals from the four BPM electrodes were amplified by four narrow band amplifiers with different gains and digitized by four independent ADCs, as shown in Fig. 6.

The highest gain channel can detect stripping with efficiency as low as $10^{-3}\%$. As the efficiency is increasing during the experiment parameter optimization, this channel is saturated, but the next channel comes out of the noise and so on, up to 100% stripping efficiency. This device proved to be extremely useful for tuning the sequential LACE process, especially after we discovered that the first laser beam converts some fraction of excited H^0 in the $n = 2$ state to protons. The mechanism of this process is simple but was overlooked when the experiment was designed. In this mechanism, the first laser beam excites the H^0 atom to the state $n = 2$, where the electron energy is too low for Lorentz stripping in the second magnet but is high enough

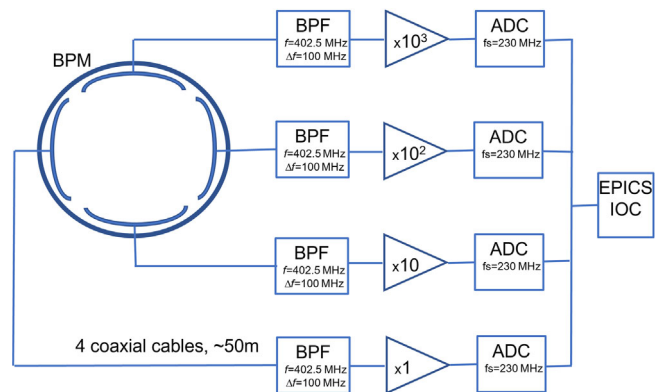


FIG. 6. A block diagram of the high-sensitivity beam current monitor HSBCM signal processor.

for the electron to be photoionized by the same laser beam. The photoionization cross section is quite small, resulting in the overall efficiency of H^- to proton conversion of $<10^{-2}\%$. Such low stripping efficiency is undetectable by the regular BCM but well within the HSBCM sensitivity range. The possibility of observing photoionization of the $n = 2$ level makes the fluorescent detector unnecessary, because the photoionization proton current is proportional to the $n = 1 \rightarrow n = 2$ excitation efficiency and can be used for tuning the first step instead of the fluorescence signal. However, the PMT is useful for alignment of the laser and ion beams, as previously described.

IV. LASER BEAM GENERATION AND DELIVERY

The overall laser system and beam delivery to the interaction point (IP) is very similar to the system described in Ref. [10] with some modifications to the previous laser system. It composed of a high-energy UV laser with 50 ns pulse width at 10 Hz repetition rate, the laser beam transport line from the laser table to the IP, and two local optical tables adjacent to the IP to control the laser beam parameters.

A. Laser system

The laser system uses a master oscillator power amplifier scheme to produce the necessary laser power and temporal structure. It consists of a master oscillator, a pulse picker, a three-stage Nd:YAG amplifier, and harmonic converters as shown in Fig. 7. The master oscillator or seeder laser is a

single-frequency narrow linewidth (<5 kHz) fiber laser with a wavelength of around 1064.5 nm with a thermal tuning range of 0.15 nm. Up to 50 mW of cw light from the seeder laser is fiber coupled to an intensity modulator unit to produce the necessary pulse structure. The intensity modulator unit uses two electro-optic lithium niobate Mach-Zehnder modulators (EOMs) to produce 50 ns pulses at 350 kHz repetition rate with a pulse contrast up to 40 dB. The intensity modulator has a bandwidth of 20 GHz or a rise time of 17.5 ps. The EOMs have dual dc bias control ports for setting up the operating point and one rf port for applying the modulation signal. To achieve an ultrahigh extinction ratio in the intensity modulation, the output power from the EOM is sampled and sent to the modulator controller. The controller constantly feeds the error signal back to the dual dc bias ports to lock the modulation signal amplitude to the null point. The repetition rate of the pulse is determined by an external electrical signal provided by an arbitrary function generator (AFG). The electrical pulses of the AFG determine the duration of the optical pulses generated by the EOMs. The shape of optical pulses is controlled by an electrical waveform shown in Fig. 8(a). The exponential-like shape of the electrical waveform is required by gain saturation occurred during amplification process which will help produce a flat pulse output. The intensity modulator output is first preamplified by a polarization-maintaining (PM) fiber amplifier (Amonics YDFA-23B-PM) before being sent to a second fiber amplifier (OptiLab YDFA-20-PM-B) that produces an average output power of 3 mW at a moderate gain setting.

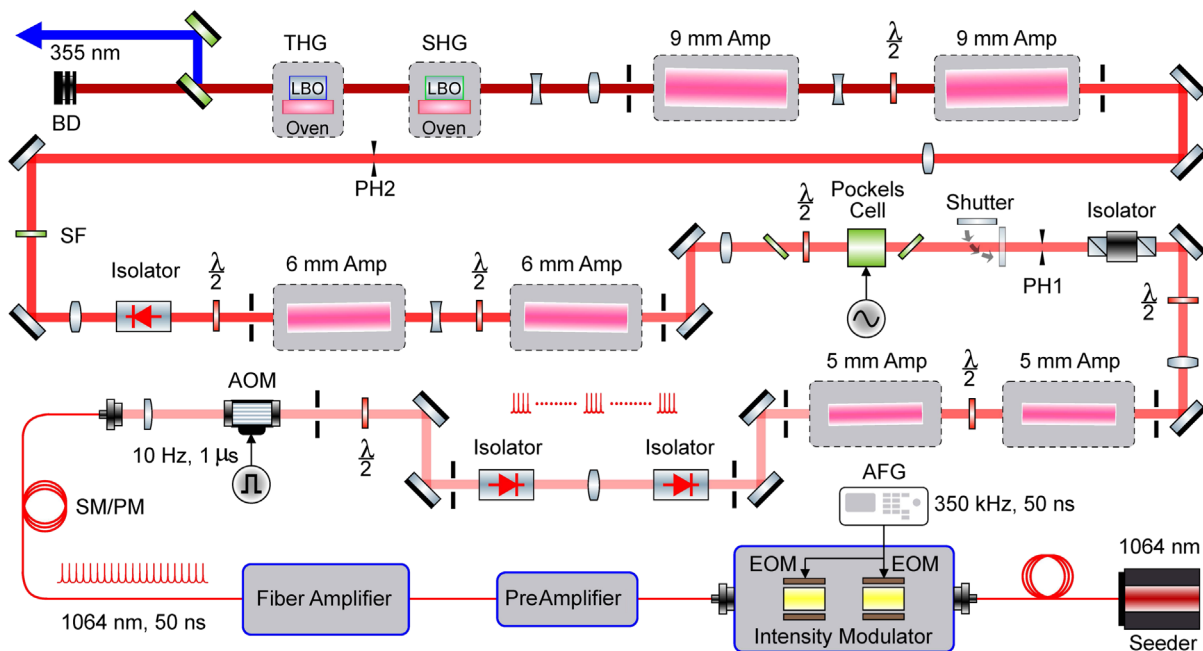


FIG. 7. Overview of the 50 ns laser system. AFG, arbitrary waveform generator; EOM, electro-optic modulator; AOM, acousto-optic modulator; $\lambda/2$, half-wave plate; SM/PM, single-mode polarization-maintaining fiber; SF, spatial filter; PH, pinhole; LBO, lithium triborate; SHG, second-harmonic generation crystal; THG, third-harmonic generation crystal; BD, beam dump.

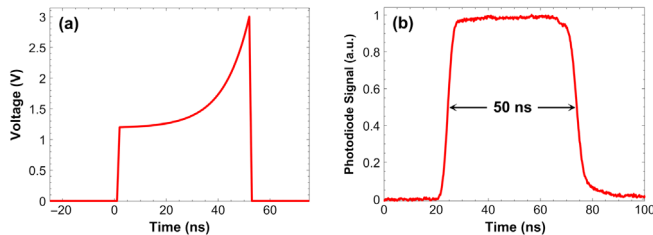


FIG. 8. (a) 50 ns control waveform on EOM. (b) A typical UV pulse waveform with 2.8 MW peak power detected by a fast photodiode.

Prior to the Nd:YAG amplifiers, the output light from the fiber amplifier is injected into a pulse picker system that uses an acousto-optic modulator (AOM) and an arbitrary waveform generator (Stanford DS345). The pulse picker reduces the repetition rate of 350 kHz pulses to produce 50 ns pulses at 10 Hz by applying 1 μ s square pulse train to the AOM at 10 Hz repetition rate. The first-order diffracted beam from the AOM provides a polarization extinction ratio in excess of 20 dB with a maximum diffraction efficiency of about 80%. Through controlling the shape of the electrical waveform from AFG, one can achieve a uniform square-shaped UV pulse at the end of the amplifiers shown in Fig. 8(b).

The power amplification scheme is very similar to the one described in Ref. [15]. It uses three-stage solid-state amplifiers, each consisting of two identical Nd:YAG rods with the diameters of 5, 6, and 9 mm, respectively. The amplifiers are pumped by eight flash lamps in total to provide about 6 orders of magnitude power amplification to the input IR pulse with about 100 nJ energy. After amplification, the output IR pulse energy is measured to be about 560 mJ (11.2 MW peak power) with a moderate voltage and pump delay settings of the last amplifier with a corresponding gain of 5.6×10^6 . This IR light is subsequently converted to its third harmonic by two lithium triborate (LBO) crystals using a pair of lenses to establish proper mode matching. With the IR input pulse energy of 560 mJ to both the second- and third-harmonic generators, the measured UV pulse energy is about 140 mJ (2.8 MW peak power) with a corresponding IR to UV conversion efficiency of about 25%. The power monitored for one-hour measurement shows about 2% rms power stability. The measured UV pulse extinction ratio after the frequency tripling is at the order of $10^5:1$ as shown in Fig. 8(b). The UV beam spatial quality is limited by both the input IR beam quality to the LBO crystals and spatial walk-offs during sum-frequency generation process. The final IR beam quality is determined by incoming IR beam quality to the Nd:YAG rods in each amplifier and the entire amplification factor. The spatial walk-off is reduced by employing a noncritical phase matching scheme using temperature-controlled ovens for both LBO crystals. The relay imaging and spatial filtering configuration in the

amplifier system (Fig. 7) is designed to help with improving the IR beam quality and, therefore, exhibits a nearly Gaussian profile at the output. The spatial UV beam profile at a peak power of 2.8 MW is shown in Fig. 10(a) with nearly TEM₀₀ Gaussian mode. Only after making sure a high-quality and stable UV laser beam is generated can it be transported to the laser ion interaction region (IP) via a long laser beam transport line.

B. Laser beam delivery

Because of scattering of the SNS high-power proton beam in the injection foil, radiation levels in the injection area are in the range of 0.8–1.0 rem/h during beam-off conditions (at 30 cm from the beam tube). To avoid this destructive radiation in the accelerator tunnel, the laser is housed in the above-ground ring service building (RSB) and propagated to a free-space laser transport line (LTL) to the experimental vessel. In order to guarantee stable and sustainable laser operation in an accelerator experiment, high-energy lasers must be located in a dust-free and temperature-stabilized area with a solid structural foundation. At the SNS, without a major disruption to neutron production operation, it is very challenging to build a dedicated laser room and transport line. Despite all these challenges, the LACE development program has been making steady progress with limited resources. The LTL was retrofitted to the existing cable chase enclosed by 6.0" diameter steel pipes that connect the laser table to the local optical table near the experimental vessel. The RSB is located 10 m above the beam line and shielded from the accelerator tunnel. The LTL itself is 60 m long, extends over two different building foundations, and contains eight relay mirrors at oblique angles with 2.0" diameter. Although its entrance and exit are sealed with 4.0" vacuum windows, it is impractical to evacuate the whole transport line. The air turbulence, humidity, and dust particle buildup from the internal wall of uncleaned cable chase severely limits quality laser beam delivery to the interaction point (IP). Moreover, conventional laser transport techniques such as relay imaging are impossible due to space constraints. Since it is also challenging to implement passive stabilization or vibration isolation to the optical boxes that are holding the mirrors, the entire LTL is susceptible to mechanical vibration especially when the accelerator is turned on, which causes laser beam jitter during the LACE experiment. A detailed description of the LTL can be found in Ref. [16].

We chose to propagate a nearly collimated laser beam using a beam expander (Thorlabs BE03-355) which produces a nearly collimated laser beam with diameters at around 7–10 mm (4σ) through the entire LTL. The transport efficiency to the IP is measured to be about 45%. The beam losses mainly come from the absorption and scattering on the mirror surfaces and air. A simplified schematic of the LACE experimental setup that includes the LTL, the RSB

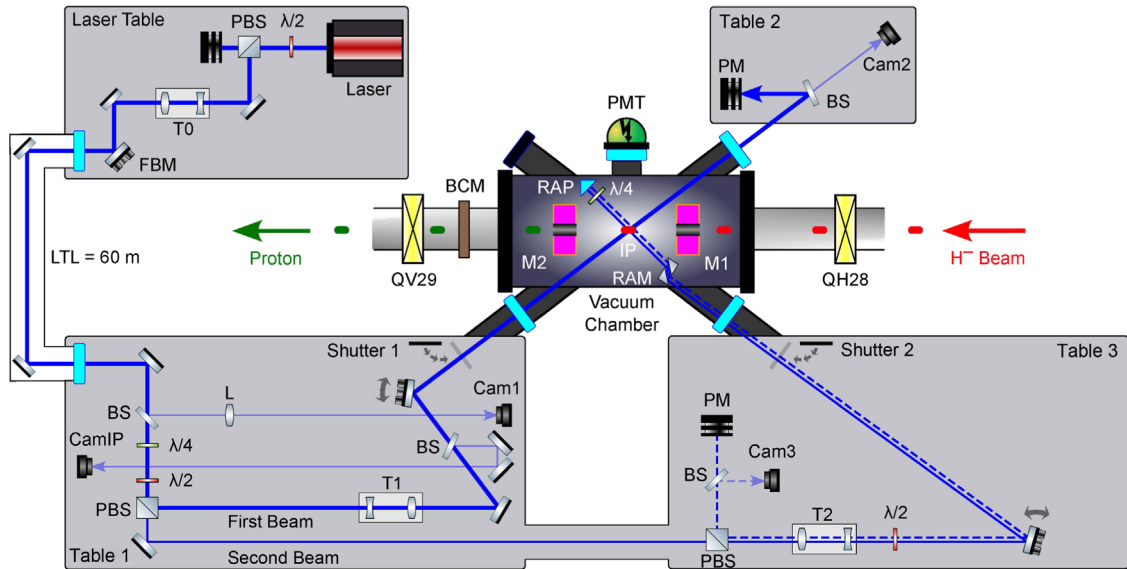


FIG. 9. Overview of the laser transport system and the experimental setup around the laser stripping chamber in the accelerator tunnel. PBS, polarized beam splitter; FBM, feedback mirror; T0–T2, telescopes; LTL, laser transport line; BS, beam splitter; PMT, photomultiplier tube; M1 and M2, magnets; QH28 and QV29, quadrupole magnets; BCM, beam current monitor; IP, interaction point; RAP, right angle prism; RAM, right angle mirror; $\lambda/2$, half-wave plate; $\lambda/4$, quarter-wave plate. The dashed lines represent the retroreflected light out of the vacuum chamber from the second beam.

laser table, and the local optical table in tunnel is shown in Fig. 9. The laser beam control optics in the RSB laser table has three main functionalities: energy tuning, beam shaping, and beam steering. The energy tuning is accomplished by combination of a half-wave plate ($\lambda/2$) and a polarized beam splitter (PBS). The beam shaping and collimating is achieved by properly tuning the beam expander (T0 in Fig. 9) to realize a nearly collimated laser beam over 65 m distance. The beam steering is achieved by using a remotely controlled piezo mirror (FBM in Fig. 9) to properly inject the laser beam to the LTL which is also used as a steering mirror for the active drift stabilization system [17].

The LACE vacuum chamber is located at about 20 m upstream of the SNS ring injection area. After the LTL, the beam is split by a polarized beam splitter (PBS) on table 1 to create the two beams required by the sequential excitation scheme of the LACE experiment. A remote controlled half-wave plate ($\lambda/2$) before the PBS in table 1 is used to control the amount of power going to each beam. The default configuration is 2/3 of the total power delivered is going to the first beam while the remaining 1/3 is used for the second beam. The quarter-wave plate ($\lambda/4$) before the $\lambda/2$ is used to compensate any depolarization during beam transport. Two remote controlled telescopes (T1 and T2) before the LACE chamber shape two laser beams to have a suitable size and divergence when they interact with the H^0 . Figures 10(b) and 10(c) show the spatial beam profiles of the first and second beam at the IP, respectively. The interaction angles of both beams are independently controlled by remote-controlled steering mirrors and stepper-motor-controlled translation stages,

respectively. Laser beam positions are monitored before and after the stripping chamber using four gigabit ethernet cameras (Allied Vision GC655), shown as cam1, cam2, cam3, and camIP in Fig. 9, by sampling the beam using four beam samplers (BSs), respectively. The sampled beam on cam1 is used to stabilize the horizontal angle of the main beam before the PBS, while the sampled beam on camIP is used to stabilize the vertical position of the first beam (entering the chamber from the left) at its IP in the feedback stabilization system. To create a copy of first beam at the IP, an image was created by splitting the beam after T1 with a BS, and camIP was placed at an equal distance from BS to IP. Using this approach, slow drifts (<1 Hz) in the laser beam are effectively eliminated, while beam jitter still dominates the inefficiencies in stripping during the experiment. The main cause of beam jitter is attributed to the mechanical vibration in the transport line and acoustic noise in the environment. The laser power allocated to the first and second beams at the IP is also remotely monitored by two ethernet-controlled power meters (PMs). Since this

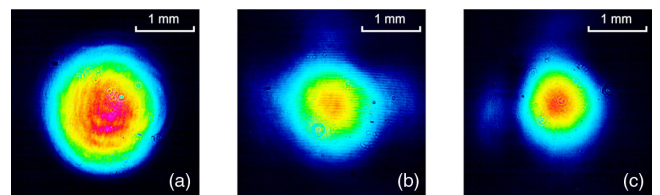


FIG. 10. (a) A spatial UV beam profile right after the laser at 2.8 MW peak power. (b) First beam profile at the interaction point. (c) Second beam profile at the interaction point.

vacuum chamber originally is not designed for the second crossing angle required by the sequential excitation scheme, a special insertion optics was designed to retrofit the vacuum chamber. The insertion optics has two main functionalities: reduce the crossing angle by about 7.1° from the vacuum chamber design angle of 142.5° and retroreflect the laser beam out of the chamber. The retroreflector is composed of two right angle mirrors (RAM), a quarter-wave plate ($\lambda/4$), and a right angle prism (RAP) as shown in Fig. 9. Additionally, there are two remote-controlled shutters located just before the entrance of vacuum chamber view ports that are used for blocking the laser beam to check the background in stripping signal. The detailed laser beam parameters during the experiment are shown in Table II.

V. EXPERIMENTAL RESULTS

After gaining sufficient experience with newly developed diagnostics and laser optics setup, a relatively straightforward procedure was established that allowed reliable setup of the sequential LACE process. (1) The SNS linac is tuned to accelerate the beam to 718.5 MeV. The beam energy is verified using the base line SNS BPM system. (2) The HEBT optics are tuned for the desired beam size at the interaction point. The beam size is verified using the wire scanner. (3) The stripping magnets are moved in, and the beam trajectory is corrected to minimize the beam loss on the stripping magnet aperture. The vertical position of the ion beam center is measured using the wire scanner. (4) The ion beam is blocked in the injector, and the first laser beam is opened. The vertical position of the laser beam is measured using the wire scanner and the PMT signal. The laser position is corrected to coincide with the ion beam position. (5) The ion beam is unblocked, and the first laser beam horizontal angle is adjusted to maximize the photoionization proton signal from the HSBCM. (6) The ion beam and the first laser beam are blocked, and the second laser beam is unblocked. The vertical position of the laser beam is measured using the wire scanner and the PMT signal. The position of the second laser is adjusted to coincide with the ion beam position. (7) The ion beam and the first laser beams are unblocked, and the second laser beam horizontal angle is adjusted to maximize the proton signal from the HSBCM. (8) At this point, typically, the proton current is within the range of the BCM. The vertical positions and horizontal angles of both laser beams are fine-tuned to achieve the maximum proton current.

If the linac and the laser operation is stable, the setup process takes about 3–4 h, which is not much longer than the single-step LACE process setup. A distribution of measured stripping efficiency during one of the experiments is shown in a histogram in Fig. 11. The maximum efficiency of 12% is close to the model prediction shown in Table II. The peak laser power split of 0.8 MW in the first

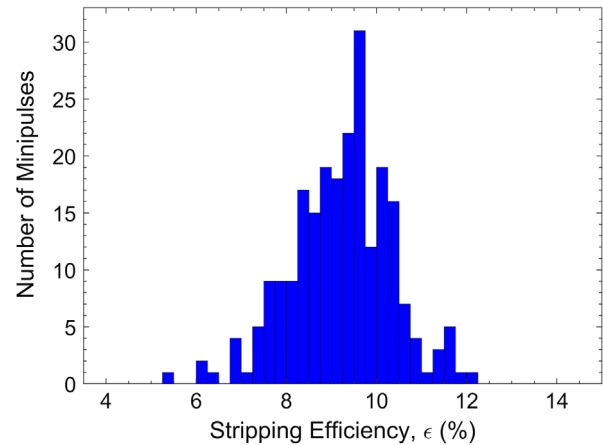


FIG. 11. A histogram of stripping efficiency distribution for multiple beam pulses.

beam and 0.5 MW in the second beam was used for this dataset. The significant spread of the data is mainly due to the laser beam vertical position and horizontal angle jitter at the interaction point.

As described in Sec. IV, the spectrum bandwidth of the cw seed laser is less than 5 kHz. The direct 50-ns pulse modulation through EOM broadens the optical spectrum to about 10 MHz based on our measurements [15]. The frequency sweeping range [8] induced by the second laser beam divergence with smaller divergence of 0.08 mrad is about 60 GHz. Therefore, the effect of the spectral bandwidth of the light source on the stripping efficiency is negligible in this experiment.

VI. SUMMARY AND FUTURE DEVELOPMENT

The sequential resonance experiment successfully confirmed the stripping scheme in agreement with model predictions. However, owing to the nonoptimal configuration of the recycled experimental vessel, many of the more attractive aspects of sequential resonance could not be explored in this experiment. For instance, high-efficiency stripping could not be achieved due to the geometric constraints of the existing vessel. Moreover, the flexibility in laser wavelength choice for each step could not be exploited due to both vessel configuration and beam energy constraints. Now that the sequential resonance stripping method has been validated experimentally; the next step in the development program is to design and build a new experimental vessel geometrically optimized for high-efficiency stripping with flexibility in the choice of laser wavelength. As with the current experimental vessel, this vessel will remain in the transport line to the accumulator ring, and, thus, stripped particles will still not be injected into the ring. The SNS beam energy will also be upgraded to 1.3 GeV within the year, extending the range of usable laser wavelengths [11]. Together, these two upgrades will allow full exploration of

the various options for production-style high-efficiency H^- stripping from single-step excitation to various sequential resonance excitation schemes with IR, green, or UV lasers. While simulations of a configuration optimized for the 1.3 GeV SNS beam predict that the total laser power required for 95% stripping efficiency is 5–6 times less for the two-step scheme [6] than for the single-step scheme, as shown here, the two-step scheme introduces additional complications in the configuration and with laser alignment. The new vessel capable of performing both schemes at high stripping efficiency will help inform decisions regarding the design of the first operational LACE ring injection system.

Along these lines, a design effort is underway to build a demonstration LACE system in the SNS injection area that will demonstrate foil-free charge exchange into an accumulator ring for the first time. Besides relieving the issues with radiation and foil sublimation, another advantage of such a system is the reduction of three beam trajectories after stripping (p , H^0 , and H^-) to two (p and H^0), as there are no remaining H^- after the first stripping magnet. This greatly simplifies transportation and disposal of the waste beam. The system will be used for demonstration and exploration of injection using a LACE system and is still one step away from a full production LACE system, which is not currently planned for SNS but may be an option.

ACKNOWLEDGMENTS

This manuscript has been authored by UT-Battelle, LLC, under Contract No. DE-AC05-00OR22725 with the U.S. Department of Energy. The U.S. Government retains, and the publisher, by accepting the article for publication, acknowledges that the U.S. Government retains a non-exclusive, paid-up, irrevocable, worldwide license to publish or reproduce the published form of this manuscript, or allow others to do so, for U.S. Government purposes. The Department of Energy will provide public access to these results of federally sponsored research in accordance with the DOE Public Access Plan [18].

APPENDIX: DISCUSSION OF THE UNCERTAINTY IN SIMULATED DATA AND THE JITTER IN THE MEASURED DATA

Stripping efficiency, both expected and experimentally observed, has some uncertainty caused by the real experiment parameters different from expected. The simulation uncertainty is derived from considering the worst and best possible combinations of laser divergence and beam energy spread parameters, whereas in the experiment these parameters are fixed and the range of stripping efficiencies comes entirely from pointing stability of the laser, which is not part of the simulation at all. More specific details are the following.

Simulations.—The simulation produces a single well-defined efficiency number for a given set of the H^- and laser beam parameters. Some of these parameters, mostly the H^- beam energy and angular spreads, are not precisely known well ahead of the experiment when the laser beam optics is tuned on the final focus optical table in the tunnel. We can tune the laser optics on the final focus table in the tunnel only during long shutdowns, which happen once or twice a year, and, therefore, we must guess the best parameters for the next run experiment. We use the best guess parameters suggested by the linac model to find the optimal value for the two laser beam divergences. The stripping efficiency calculated for these parameters is the best we expect to achieve and represents the upper limit in the efficiency range (0.15 in Table II). We know from linac operational experience that the beam energy spread can deviate significantly from the design value when the linac is tuned for minimum losses in the beginning of each run. To calculate the lowest efficiency in the range, we assume the worst-case combination of the maximum beam energy spread we can expect, together with a laser beam divergence optimized for a different beam energy spread. This number represents the lowest limit in the efficiency range (0.03 in Table II). The best efficiency achieved in the experiment of 0.12 is close to the upper end of the expected range, which means the ion beam parameters were close to the design values and the laser beam divergence is close to optimal.

Experiment.—The nature of the stripping efficiency spread is much simpler. The width of the spread depends on how well the laser stabilization system works. When the laser position feedback is off, we see the stripping efficiency covering the whole range from 0 to 0.12. The lowest number of 0.05 in the histogram in Fig. 11 is just a coincidence of the feedback tuning for this particular set and the total number of shots collected. For better tuned feedback, this number could be larger and with more points in the statistics, and we could see smaller numbers for rare unfortunate laser shots.

In principle, it would be interesting to derive the frequency vs angle dependencies shown in Fig. 2 using the laser jitter as a sampling tool. Unfortunately, the excitation efficiency dependence on the crossing angle is masked by the laser beam divergence. We set the divergence large enough to mitigate the effects of the horizontal angle spread due to finite horizontal beam emittance and the beam energy spread due to finite longitudinal beam emittance. The laser vertical position jitter seems to be the dominant source of the stripping efficiency jitter. Histograms in Figs. 12 and 13 show single-step and sequential excitation jitter. The width of the spread is comparable for the two schemes and strongly depends on the laser position feedback tuning. The jitter effect and mitigation is discussed in depth in Ref. [17].

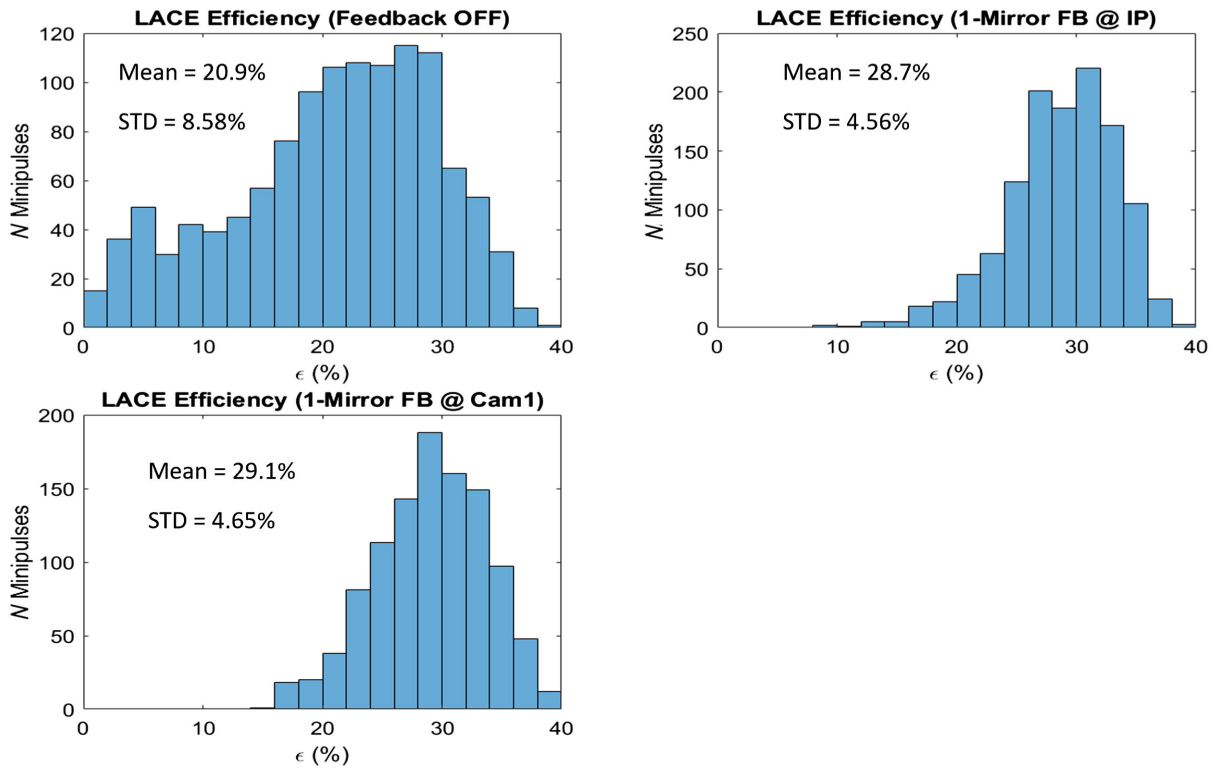


FIG. 12. A histogram of the stripping efficiency in the single-step excitation experiment for different conditions of the laser positioning feedback. Top left: The feedback is off. Top right: The feedback is on but not optimized. Bottom left: All parameters are optimally tuned.

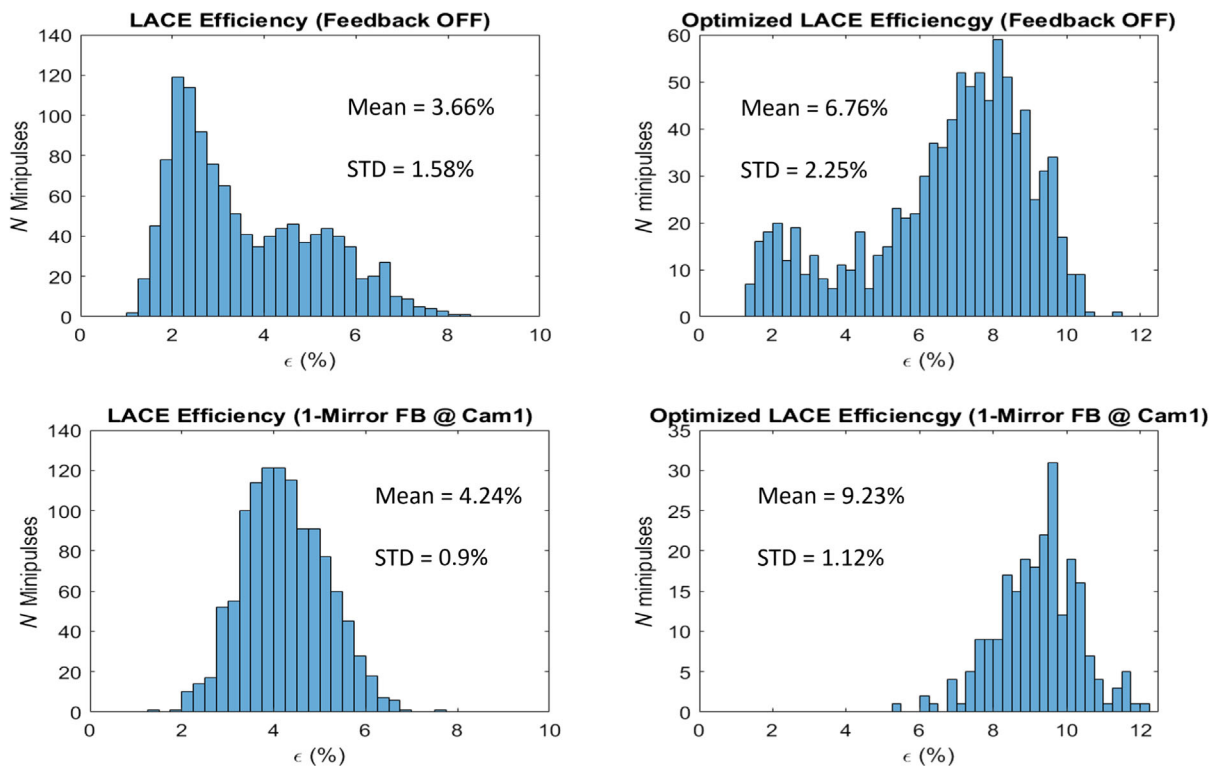


FIG. 13. A histogram of the stripping efficiency in the sequential excitation experiment for different conditions of the laser positioning feedback. Top left: The feedback is off. Top right: The feedback is off, but the laser beams are aligned. Bottom left: The feedback is on, but the laser beams are not well aligned. Bottom right: The feedback is on, and the laser beams are optimally aligned.

- [1] L. W. Alvarez, *Rev. Sci. Instrum.* **22**, 705 (1951).
- [2] M. Plum, H[−]—charge exchange injection issues at high power, in *Proceedings of the HB2016 conference, Malmo, Sweden* (2016), p. 304.
- [3] N. Evans, Foil R&D and temperature measurements at the SNS, in *Proceedings of the NAPAC2019 conference, Lansing, MI, 2019* (2019).
- [4] T. Kanemura, M. LaVere, R. Madendorp, F. Marti, T. Maruta, Y. Momozaki, P. N. Ostroumov, A. S. Plastun, J. Wei, and Q. Zhao, Experimental Demonstration of the Thin-Film Liquid-Metal Jet as a Charge Stripper, *Phys. Rev. Lett.* **128**, 212301 (2022).
- [5] P. Saha, H. Harada, S. Kato, M. Kinsho, Y. Irie, and I. Yamane, An experimental plan for 400 MeV H[−]—stripping to proton by using only lasers in the J-PARC RCS, in *Proceedings of the HB2016 conference, Malmo, Sweden* (2016), p. 310.
- [6] T. Gorlov, A. Aleksandrov, S. Cousineau, Y. Liu, A. Oguz, M. Kay, and P. Saha, Laser stripping for 1.3 GeV H[−]—beam at the SNS, in *Proceedings of the NAPAC2022 conference, Albuquerque, NM* (2022).
- [7] S. Henderson, W. Abraham, A. Aleksandrov, C. Allen, J. Alonso, D. Anderson, D. Arenius, T. Arthur, S. Assadi, J. Ayers, P. Bach, V. Badea, R. Battle, J. Beebe-Wang, B. Bergmann, J. Bernardin, T. Bhatia, J. Billen, T. Birke and E. Bjorklund *et al.*, The spallation neutron source accelerator system design, *Nucl. Instrum. Methods Phys. Res., Sect. A* **763**, 610 (2014).
- [8] V. Danilov, A. Aleksandrov, S. Assadi, J. Barhen, W. Blokland, Y. Braiman, D. Brown, C. Deibele, W. Grice, S. Henderson, J. Holmes, Y. Liu, A. Shishlo, A. Webster, and I. N. Nesterenko, Proof-of-principle demonstration of high efficiency laser-assisted H[−] beam conversion to protons, *Phys. Rev. Accel. Beams* **10**, 053501 (2007).
- [9] S. Cousineau, A. Rakhman, M. Kay, A. Aleksandrov, V. Danilov, T. Gorlov, Y. Liu, M. Plum, A. Shishlo, and D. Johnson, First Demonstration of Laser-Assisted Charge Exchange for Microsecond Duration H[−] Beams, *Phys. Rev. Lett.* **118**, 074801 (2017).
- [10] S. Cousineau, A. Rakhman, M. Kay, A. Aleksandrov, V. Danilov, T. Gorlov, Y. Liu, C. Long, A. Menshov, M. Plum, A. Shishlo, A. Webster, and D. Johnson, High efficiency laser-assisted H[−] charge exchange for microsecond duration beams, *Phys. Rev. Accel. Beams* **20**, 120402 (2017).
- [11] T. Gorlov, A. Aleksandrov, S. Cousineau, Y. Liu, A. Rakhman, and A. Shishlo, Sequential excitation scheme for laser stripping for a H[−] beam, *Phys. Rev. Accel. Beams* **22**, 121601 (2019).
- [12] V. Danilov, A. Aleksandrov, S. Assadi, S. Henderson, N. Holtkamp, T. Shea, A. Shishlo, Y. Braiman, Y. Liu, J. Barhen, and T. Zacharia, Three-step H[−] charge exchange injection with a narrow-band laser, *Phys. Rev. Accel. Beams* **6**, 053501 (2003).
- [13] T. Gorlov and A. Shishlo, in *Proceedings of the ICAP2009* (2009).
- [14] T. Gorlov, V. Danilov, and A. Shishlo, Laser-assisted H[−] charge exchange injection in magnetic fields, *Phys. Rev. Accel. Beams* **13**, 050101 (2010).
- [15] C. Huang, C. Deibele, and Y. Liu, Narrow linewidth picosecond UV pulsed laser with mega-watt peak power, *Opt. Express* **21**, 9123 (2013).
- [16] Y. Liu, A. Rakhman, A. Menshov, A. Webster, T. Gorlov, A. Aleksandrov, and S. Cousineau, Laser and optical system for laser assisted hydrogen ion beam stripping at SNS, *Nucl. Instrum. Methods Phys. Res., Sect. A* **847**, 171 (2017).
- [17] M. Kay and A. Oguz, Pointing stabilization of 140 mJ, 10 Hz UV laser for laser-assisted charge exchange (to be published).
- [18] <http://energy.gov/downloads/doe-public-access-plan>.